IEEE Access
Multidisciplinary | Rapid Review | Open Access Journal

Received April 3, 2018, accepted May 7, 2018, date of publication May 14, 2018, date of current version June 5, 2018.

Digital Object Identifier 10.1109/ACCESS.2018.2835815

Ultra-Wideband Microwave Absorption by Design and Optimization of Metasurface Salisbury Screen

ZIHENG ZHOU[1], KE CHEN[1], (Member, IEEE), BO ZHU[1], (Member, IEEE), JUNMING ZHAO[1], (Member, IEEE), YIJUN FENG[1], (Member, IEEE), AND YUE LI[2], (Senior Member, IEEE)

[1]Department of Electronic Engineering, School of Electronic Science and Engineering, Nanjing University, Nanjing 210093, China
[2]Department of Electronic Engineering, Tsinghua University, Beijing 100084, China

Corresponding authors: Ke Chen (ke.chen@nju.edu.cn) and Yijun Feng (yjfeng@nju.edu.cn)

This work was supported in part by the National Nature Science Foundation of China under Grants 61731010, 61671231, and 61571218, in part by the China Postdoctoral Science Foundation funded project under Grant 2017M620202, in part by the Fundamental Research Funds for the Central Universities, in part by PAPD of Jiangsu Higher Education Institutions, and in part by the Jiangsu Key Laboratory of Advanced Techniques for Manipulating Electromagnetic Waves.

ABSTRACT In this paper, we have designed an ultra-wideband electromagnetic (EM) absorber based on the concept of metasurface Salisbury screen (MSS), which features low profile, light weight, simple configuration, and robust angular performance. The metasurface with extremely simple patch pattern is utilized to generate diverse controllable reflection phases, in place of the non-dispersive metallic plate used in conventional absorbers, thus achieving a multi-octave ultra-wideband EM wave absorption. Equivalent circuit model is established to analyze the performance of the MSS elements, and then the genetic algorithm and simulated annealing algorithm are employed to optimize the MSS element geometries and their spatial distribution. The proposed and fabricated MSS, with a polarization-insensitive absorption over 88% from 3.74 to 18.5 GHz verified by experiments, shows a considerable bandwidth improvement compared with the conventional Salisbury screen of same thickness which has 88% absorption band from 4.8 to 11.5 GHz. Furthermore, the MSS can still provide ultra-wideband absorption with high efficiency for large incident angle, for example, higher than 82% for 45° incidence. The proposed concept could provide opportunities for flexibly designing ultra-wideband EM absorbers, exhibiting promising potentials for many practical applications, such as electromagnetic compatibility, stealth technique, and so on.

INDEX TERMS Metasurface, wide-band microwave absorber, optimization algorithm, Salisbury screen.

I. INTRODUCTION

As the essential devices for efficient electromagnetic (EM) power absorption, EM absorbers [1]–[6] play an important role in numerous applications from radio to terahertz and optical frequencies, such as electromagnetic compatibility, stealth technology, imaging and sensing, etc. Dallenbache layer [7], [8] or Salisbury screen [7]–[11] are classical designs employed in microwave region, predominantly as an efficient mean to reduce the radar visibility of targets. The Dallenbache layers using lossy magnetic or dielectric materials can provide a remarkable multi-octave absorption bandwidth, but the large mass density inherently limits their uses in many circumstances. The conventional Salisbury screen (CSS) has a single homogeneous resistive sheet placed quarter-wavelength distance from the metal ground. Although the CSS is highly appreciated for its appealing light-weight structure and extremely simple geometry, the narrow bandwidth performance and discrete resonating absorption peaks are still the problems. Therefore, many possible methods are proposed to improve the bandwidth performance of the CSS: Jaumann screen [11]–[14] absorbers using multilayered configurations; circuit analogous (CA) absorbers [15]–[18] comprising resistive frequency selective surfaces (FSS) [18]; high-impedance surface (HIS) based Salisbury screen with an additional narrow absorption band closely depending on the EM behavior of the HIS [19], [20]. The emergence of metamaterials caused an upsurge of metamaterial absorber research, due to that these artificially composite particles can emulate many materials' EM responses not available with natural occurring materials [1], [2], [21], [22]. To improve the absorption bandwidth, metamaterial absorbers are often loaded with chip resistors or using metal/dielectric

multilayered geometries, which can efficiently dissipate the impinging EM waves with broad absorption bandwidth, but the assembly procedures might be quite complex and time-consuming since they usually require careful soldering and precise layer alignments [23]–[26]. As we shall see, the most practical problem for EM absorber with a given thickness is to maximally improve the efficient absorption bandwidth. Other crucial issues are associated with the weight, the complexity of design and fabrication, and the sensitivity of absorption on the polarization and incidence angle of the incident EM waves. Though considerable efforts have been made to develop wideband microwave absorbers, they could seldom simultaneously solve all these problems together, and new practical deployable solutions are still necessary.

As a class of structured surfaces, metasurfaces are able to fully control the wavefront either in reflection or transmission operation by introducing abrupt phase changes, which have been implemented in applications such as beam shaping [27], polarization transform [28], [29], absorption enhancement [30], flat lensing [31], [32], wave coupling [33], and invisibility cloaking [34], etc. In our previous work [35], by using metasurface ground, the concept of metasurface Salisbury screen (MSS) is proposed and proved as a promising way to realize ultra-wideband microwave absorber with simultaneously light weight, low profile, and robust angular performance. The metasurface with designable spatial phase response and spatial arrangement is employed to serve as the ground for the generation of multiple resonances. As demonstrated, nearly 8.2 dB reflection reduction from 6 GHz to 30 GHz can be obtained. This wideband absorption performance closely depends on the metasurface ground, which is composed of several kinds of elements that should be independently optimized using time-consuming full-wave simulation.

Here in this paper, compared with the previous work, full theoretical analysis is proposed to automatically optimize the metasurface elements and the MSS absorption performance, which do not have reliance on the full-wave simulation during the whole design process, showing a much less time-consuming and effort-costing analytical approach for designing MSS. The analytical model can be extended to oblique case and give insight to the underlying mechanism of the robust angular performance of MSS, which was not studied in [35]. In addition, the MSS has a simpler configuration composed of only patch-patterned elements but with a higher absorption performance working in lower microwave band that covers the entire C-band (4 GHz - 8 GHz), X-band (8 GHz - 12 GHz), and Ku-band (12 GHz - 18 GHz). Guided by equivalent circuit analysis [36], we establish an analytical model to extract the reflection response of the MSS either under normal or oblique incidence. Furthermore, a systematic optimization method is established to obtain the optimal backward radar cross section (RCS) reduction and uniformly suppress scatterings in the whole backward half-space. The theoretical results are compared with the full-wave simulations and experiments, which shows relatively good agreement among them. These results have demonstrated that ultra-wideband (3.74 GHz - 18.5 GHz) absorption over 88% can be achieved by the proposed MSS, showing a great advantage over the CSS of same thickness which has an 88% absorption band from 4.8 GHz to 11.5 GHz. In addition, the metasurface can reduce the sensitivity of the resonance modes on the incidence angle. As a result, the absorption with slightly reduced efficiency can be achieved in the operation band for large incident angles.

The rest of the paper is organized as follows. Section II compares the resonant features of the CSS and MSS, and gives the general design principle of the MMS. In Section III, a general analytical circuit model of the MSS element is set up to quantitatively analyze the MSS resonance, and specially to analyze the MSS element based on patch-patterned meta-atom in detail. Optimization procedure for achieving the best absorption performance within a given frequency band is presented in Section IV. Section V shows the simulated and measured results of the ultra-wideband absorption by the proposed MSS. Finally, Section VI summarizes the paper.

II. COMPARISON BETWEEN THE CSS AND THE MSS ON RESONANT PRINCIPLE

Figure 1(a) illustrates the schematic of the CSS with intrinsically simple geometry, which has a resistive sheet with surface impedance of 377Ω/□ suspended above the metallic ground plate by a distance of l. At normal incidence case, Salisbury screen resonance can be trigged when the whole phase accumulation as the EM wave interacts with the CSS reaches $2n\pi$:

$$4\pi f_n\, l/c - \pi = 2n\pi \tag{1}$$

where $n = 0, 1, 2\ldots$ corresponds to its n^{th} order resonance, respectively. Since the metallic ground has an intrinsic constant reflection phase of π, the necessary phase accumulation for Salisbury resonance can be only satisfied at certain frequencies, resulting in discrete and narrow absorption bands, as schematically illustrated in Fig. 1(b).

The key to manipulate the Salisbury screen resonance lies on the reflection phase of the bottom ground plane. Different to metallic ground with constant reflection property in microwave region, metasurfaces are capable of generating arbitrary spectral reflection phases in a desirable manner, which have been already been demonstrated by numerous existing works [37], [38]. In Fig. 1(c), the metallic ground of CSS is replaced by the reflective metasurface consisting of several kinds of meta-atoms with distinct phase responses. As a result, Fig. 1(d) shows that the different Salisbury screen resonances can be generated successively distributed along the frequency axis, enabling a continuously wideband absorption performance. The required elements can be easily realized by patterning with different surface textures. This type of MSS resonance is the collective result of the air spacer and the resonance of reflective meta-atoms, which can be custom-designed with arbitrary operation frequencies while maintaining the spacing distance unchanged. Such a

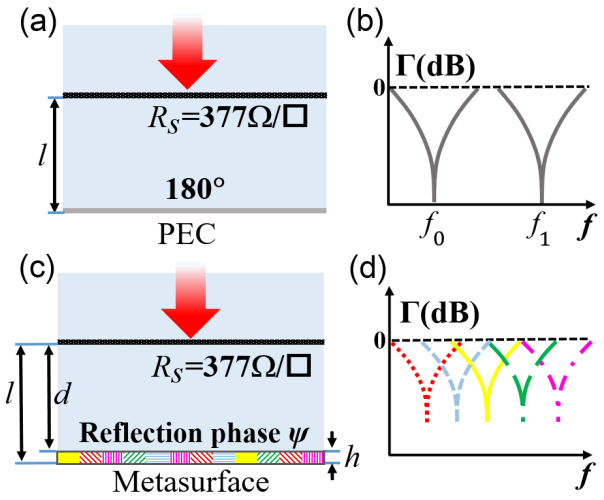

FIGURE 1. (a) The configuration of a CSS with total thickness of *l*, and (b) the reflection response. (c) The configuration of MSS based on the metasurface composed of several kinds of meta-atoms, and (d) the corresponding reflection response. The total thickness of the MSS structure is *l*. The thickness of the metasurface is *h* and the distance between the metasurface and the resistive sheet is *d*.

resonance is quite different to that of CSS, of which the resonant mode is solely determined by the spacer thickness.

The reflection properties of these elements can be elaborately optimized to realize many MSS resonant modes with almost equal distribution across the pre-designed frequency band. Therefore, these multiple and closely distributed resonances can lead to an ultra-wideband microwave absorption. Since continuously ultra-wideband EM absorption is more appreciable for practical applications [39], the MSS would be much attractive due to that the new degrees of freedom introduced by the metasurface could allow a large controllability and improvement of the absorption bandwidth.

III. THE MSS ELEMENT ANALYSIS VIA THE EQUIVALENT CIRCUIT METHOD

The equivalent circuit model is employed to quantitatively interpret the relationship between the resonant modes of the MSS element and the reflection response of the meta-atom. The MSS element is constructed by the top resistive sheet layer with surface impedance of $R_s = \eta_0 = 377\Omega/\square$ and the bottom meta-atom layer, with the middle air spacer being a thickness of d, as shown in Fig. 2(a). Figure. 2(b) illustrates the equivalent circuit model of the MSS element with the incident angle of α. The meta-atom here is regarded as a lossless load Z_L since the little loss in metasurface can be ignored. The air spacer behaves as a section of transmission line with propagation constant $\beta_0 = (\omega/c)\cos(\alpha)$ and intrinsic impedance Z_0, which equals $\eta_0/\cos(\alpha)$ for TE-polarized incidence and $\eta_0\cos(\alpha)$ for TM case. The resistive sheet is viewed as a resistor in the circuit model. The reflection of the meta-atom can be related to its reflection phase response $\psi(f)$, and given as:

$$\frac{Z_L - Z_0}{Z_L + Z_0} = e^{j\psi(f)} \tag{2}$$

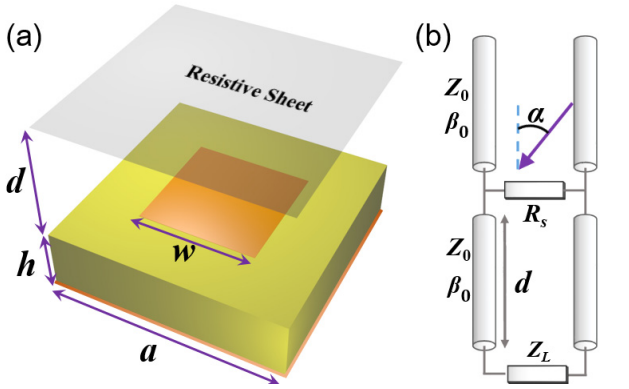

FIGURE 2. (a) Schematic of the MSS element. The side length of the patch is denoted by *w*. The unit periodicity *a*, substrate thickness *h*, and the spacing distance *d* are 12 mm, 3 mm, and 6 mm, respectively. (b) The equivalent circuit model of the MSS element.

Through some analytical manipulations, we can obtain the reflection of the MSS element:

$$\Gamma_{\mathrm{TE}} = \frac{2\cos(\alpha) - 1 - e^{j(2\beta_0 d - \psi(f))}}{(2\cos(\alpha) + 1)e^{j(2\beta_0 d - \psi(f))} + 1} \tag{3-a}$$

$$\Gamma_{\mathrm{TM}} = \frac{2 - \cos(\alpha)e^{j(2\beta_0 d - \psi(f))} - \cos(\alpha)}{(2 + \cos(\alpha))e^{j(2\beta_0 d - \psi(f))} + 1} \tag{3-b}$$

For the normal incidence ($\alpha = 0$), the above equation can be reduced to:

$$\Gamma = \frac{1 - e^{j(2\beta_0 d - \psi(f))}}{3e^{j(2\beta_0 d - \psi(f))} + 1} \tag{4}$$

The reflection coefficient will vanish ($\Gamma = 0$) when the following resonance condition

$$4\pi f_n d/c - \psi(f_n) = 2n\pi, \quad n = 0, 1, 2\ldots \tag{5}$$

is satisfied. Hence, the spectral absorption peaks can be flexibly designed by manipulating the reflection phase of the metasurface. In addition, by increasing the variation rate of $\psi(f)$, both the fundamental MSS resonance ($n = 0$) and high-order modes can be excited in the pre-designing frequency band, further reducing the intervals between two neighboring MSS resonances.

The meta-atom with readily controllable phase response is crucial for the design of MSS. In this scheme, the meta-atom with square patch pattern is chosen due to its simplicity in design, analysis and fabrication, as shown in Fig. 2(a). The input impedance of such meta-atom for TE- and TM-polarized incidence can be calculated analytically by [40]:

$$Z_{\mathrm{TE}} = \frac{j\omega\mu_0 \frac{\tan(\beta h)}{\beta}}{1 - 2k_{eff}\gamma\frac{\tan(\beta h)}{\beta}(1 - \frac{\tan(\beta h)}{\beta})} \tag{6-a}$$

and

$$Z_{\mathrm{TM}} = \frac{j\omega\mu_0 \frac{\tan(\beta h)}{\beta}(1 - \frac{\sin^2(\alpha)}{\varepsilon_r})}{1 - 2k_{eff}\gamma\frac{\tan(\beta h)}{\beta}(1 - \frac{\sin^2(\alpha)}{\varepsilon_r})} \tag{6-b}$$

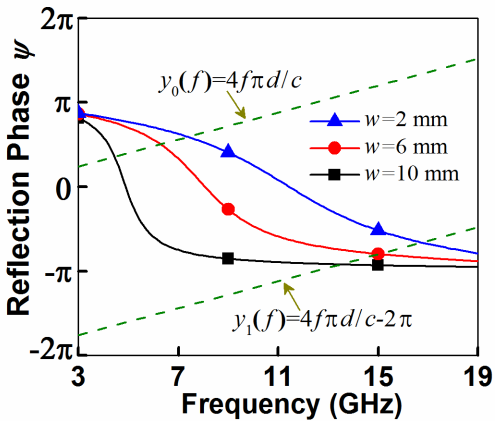

FIGURE 3. The reflection phase responses of the meta-atoms with different parameter w. According to Eq. 3, the resonance frequencies of the MSS are the intersections of the dashed lines $y_n(f) = 4f\pi d/c - n\pi$ and the reflection curves of the meta-atoms.

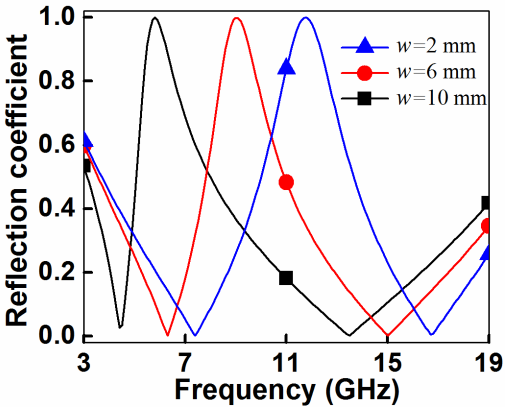

FIGURE 4. The reflection coefficients of the MSS elements based on the meta-atoms with different parameters w.

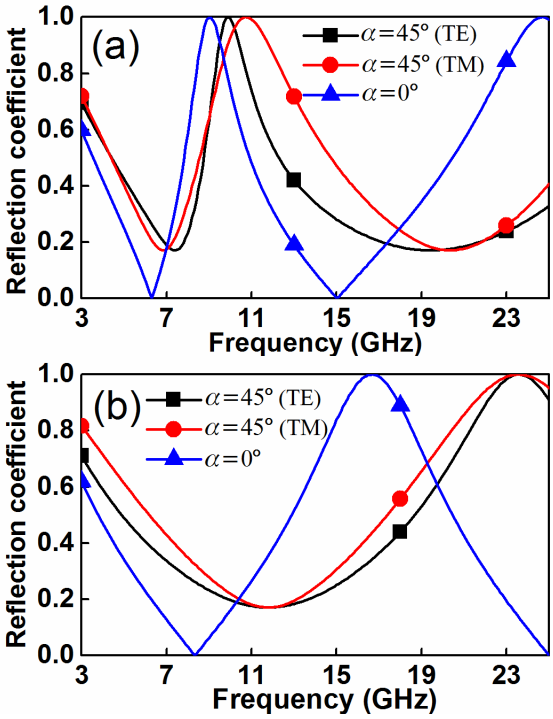

FIGURE 5. The reflection coefficient of (a) the MSS element with $w = 6$ mm, and (b) the CSS under the normal incidence and oblique incidence with incident angle $\alpha = 45°$.

where $\beta = \sqrt{k_0^2\varepsilon_r - k_t^2}$ is the normal component of the wave vector in the substrate, $k_t = k_0 \sin(\alpha)$ is the tangential component of the wavenumber, h is the height of the grounded dielectric substrate, $k_{eff} = k_0\sqrt{\varepsilon}_{eff}$ is the wave number in the effective host medium, $\varepsilon_{eff} = (\varepsilon_r + 1)/2$ is the effective relative permittivity of the host medium, ε_r is the relative permittivity of the substrate, and α is the incident angle. The grid parameter γ for array of ideally conducting patches reads:

$$\gamma = -\frac{k_{eff}a}{\pi}\ln(\sin\frac{\pi(a-w)}{2a}) \tag{7}$$

where a is the unit cell size and w represents the side length of the patch. The unit cell size a is 12 mm while the distance between the resistive sheet and the meta-atom is $d = 6$ mm. As an example, the thickness of the dielectric substrate is selected as $h = 3$ mm with a relative permittivity of 4.3 and loss tangent of 0.002.

We first investigate the normal incidence case. The frequency-dependent reflection phase responses of the meta-atoms with different parameters w are calculated by equations (2) and (6), and the curves are depicted in Fig. 3. According to Eq. 5, the MSS resonance occurs when the curves of the meta-atoms' reflection phase intersect with the lines $y_n(f) = 4f\pi d/c - 2n\pi, n = 0, 1, 2\ldots$ (Dashed lines in Fig. 3). The corresponding reflection coefficient of each MSS element can be derived from equation (4), and the results are shown in Fig. 4. Resonances of order $n = 0$ and $n = 1$ can be simultaneously excited within the frequency band of interest. In addition, via a change of the parameter w, we can gradually adjust the two resonant frequencies, offering a flexibly control of the MSS resonance, which will further benefit the element optimization and the array synthesis of the metasurface in the next section.

Then it follows the analysis of reflection responses of the MSS elements at oblique incident case with different incident angle α and wave polarizations. Figure 5 shows the theoretical results of the MSS element with $w = 6$ mm under the incident angle $\alpha = 45°$ for TE and TM polarizations. At large incident angle, the impedance between the free space and the MSS cannot be perfectly matched at the resonant frequency, leading to the reflection coefficient at each dip being no longer vanished to zero but reduced to a small value about 0.2. It is clearly observed from the theoretical results that the resonant frequency of the first MSS resonance is quite insensitive to the change of incident angle for both TE and TM polarizations, which could ensure a relatively good absorption performance in low frequency region even for large incident angles. Although the second

MSS resonance shifts towards higher frequency as the incident angle increases, the bandwidth defined by the reflection coefficient below 0.3 (-10 dB) keeps nearly unchanged for TM polarization and even being broadened for TE polarization (as shown in Fig. 5). Therefore, by combining several kinds of MSS elements in one design, it is possible to achieve continuously ultra-wideband absorption with stable angular performance. As the comparison, the resonant peak of the CSS undergoes a more obvious blue-shift at oblique incidence, resulting in a less stable angular performance especially in low frequency region.

IV. DESIGN OF AN MSS VIA OPTIMIZATION ALGORITHMS

Now we consider a design example of 10 × 10 array composed of five types of reflective MSS elements with different geometric parameters w_i ($i = 1, 2, 3, 4, 5$), aiming to realize an absorption covering from 4 GHz to 18 GHz. Since the overall absorption performance of the MSS is attributed to the multiple resonances of MSS elements, the proportion of the MSS elements as well as their spatial distributions should be seriously optimized. Based on the aforementioned analytical models, here we develop a systematic method to optimize out the best performance of the MSS. We first derive the equivalent electric and magnetic currents on MSS induced by the incoming wave at an incident angle α. Then, the far-field scattering of the MSS is calculated through a method similar to the classic theory of phased array, where each MSS element is equivalent to an EM surface source with certain initial amplitude and phase [41]. After some manipulation, the scattered electric field from MSS exposed to the incidence with TE and TM polarization can be obtained respectively:

$$\begin{aligned}\overrightarrow{E_s} = {} & jk(\cos(\varphi)\,(\cos(\theta)\cos(\alpha)+1)\,\hat{\theta} \\ & -\sin(\varphi)\,(\cos(\theta)+\cos(\alpha))\,\hat{\varphi}) \\ & \cdot \sum\nolimits_{p,q} \frac{\Gamma_{p,q}E_0 e^{-jkr}}{4\pi r} I(\theta,\varphi,\alpha,p,q) \end{aligned} \tag{8-a}$$

and

$$\begin{aligned}\overrightarrow{E_s} = {} & -jk(\sin(\varphi)(\cos(\theta)+\cos(\alpha))\hat{\theta} \\ & +\cos(\varphi)(\cos(\theta)\cos(\alpha)+1)\hat{\varphi}) \\ & \cdot \sum\nolimits_{p,q} \frac{\Gamma_{p,q}E_0 e^{-jkr}}{4\pi r} I(\theta,\varphi,\alpha,p,q) \end{aligned} \tag{8-b}$$

where E_0 is the electric field amplitude of the incidence, k is the wave number, r denotes the observational radius in far-field region, $\Gamma_{p,q}(f)$ represents the complex reflection coefficient of the MSS element located at (pa, qa), and I(θ, φ, α, p, q) is an element function of angle θ, azimuth angle φ, and incidence angle α [35]:

$$\begin{aligned}&\mathrm{I}(\theta,\varphi,\alpha,p,q) \\ &= \int_{qa}^{(q+1)a}\int_{pa}^{(p+1)a} e^{jk(\sin(\theta)\cos(\varphi)x'+\sin(\theta)\sin(\varphi)y'+\sin(\alpha)y')}\,\mathrm{d}x'\,\mathrm{d}y' \end{aligned} \tag{9}$$

First consider the normal incidence ($\alpha = 0°$), the backward RCS ($\theta = 0°$) of the MSS calibrated to the same-sized metallic plate reduces to $20\lg(\left|\sum_{i=1}^{5} x_i \cdot \Gamma(f; w_i)\right|)$, where $\Gamma(f; w_i)$ is the frequency-dependent reflection coefficient of the MSS element with the patch side length w_i, and x_i corresponds to its proportion. To achieve the lowest backward reflection in the pre-designed frequency band, we employ the genetic algorithm (GA) [42], [43] to optimally choose the parameters w_i and x_i. The GA can mimic the processes of procreation in nature by the genetic operators of selection, crossover, mutation and evaluation. It starts with a randomly selected population of potential solutions and then gradually evolves towards improved solutions, and finally outputs with the global optimized result. We are aimed to inhibit the backward reflection over the whole working band, which means the maximum reflection within the prescribed bandwidth should be as minor as possible. The defined objective function and the constraint conditions are:

$$\begin{aligned}\mathrm{G}\left(\vec{w},\vec{x}\right) = {} & \mathrm{Max}\{20\lg(|\sum\nolimits_i x_i \cdot \Gamma(f; w_i)|), f \in (f_l, f_h)\} \\ & 0 \le x_i \;\&\; \sum\nolimits_i x_i = 1 \;\&\; 0 \le w_i \le a, \end{aligned} \tag{10}$$

where $\vec{w}$ represents the array (w_1, w_2, w_3, w_4, w_5) and $\vec{x}$ represents the array (x_1, x_2, x_3, x_4, x_5). The lower and upper bounds of pre-designed frequency f_l and f_h are set as 4 GHz and 18 GHz, respectively. The optimization program was carried out by a computer with the i5-Intel Core and 4 GB memory. The objective function at each generation of evolution is illustrated in Fig. 6. The global optimum of -9.7 dB RCS reduction can finally be achieved within 40 generations which takes about 30 minutes, and the optimal solution for $\vec{w}$ and $\vec{x}$ are obtained as {0 mm, 4.039 mm, 7.23 mm, 9.506 mm, 11.203 mm} and {21.9%, 19.3%,19.6%, 20.3%, 18.9%}, respectively. We should emphasize that no full-wave numerical calculation is involved in the optimization as we use the simple patch elements in the metasurface which have analytical formulas for reflection calculation, thus it largely reduces the whole computing time. The design scheme is not limited to 10 × 10 array and 4-18 GHz, and MSS using patch-patterned elements and other-scaled arrays (6 × 6, 8 × 8, 15 × 15, etc.) can be directly developed for specific uses, for example, EMC in communication system or absorption requirement in other frequency regime.

In the above optimization, the backward reflection can be well suppressed in an ultra-wide band by optimizing the proportion of each element. However, the spatial distribution of the MSS elements should be optimized as well to avoid high side lobes in the backward half-space. Here, we use the simulated annealing algorithm to obtain the optimal arrangement of MSS element for reducing the side-lobe level as small as possible [44], [45]. Details of this procedure can be found in [35]. Five types of MSS elements with different patch sizes w of 0 mm, 4.039 mm, 7.23 mm, 9.506 mm and 11.203 mm are denoted by the number of "1", "2", "3", "4", and "5", respectively. The initial arrangement is represented by the

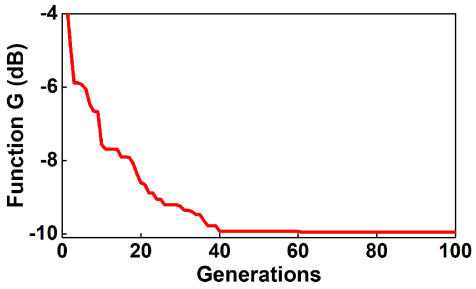

FIGURE 6. The objective function of the GA algorithm as a function of evolution generation.

following matrix:

$$\begin{bmatrix} 1 & 1 & 1 & 1 & 1 & 1 & 1 & 1 & 1 & 1 \\ 1 & 1 & 1 & 1 & 1 & 1 & 1 & 1 & 1 & 1 \\ 1 & 2 & 2 & 2 & 2 & 2 & 2 & 2 & 2 & 2 \\ 2 & 2 & 2 & 2 & 2 & 2 & 2 & 2 & 2 & 2 \\ 2 & 2 & 3 & 3 & 3 & 3 & 3 & 3 & 3 & 3 \\ 3 & 3 & 3 & 3 & 3 & 3 & 3 & 3 & 3 & 3 \\ 4 & 4 & 4 & 4 & 4 & 4 & 4 & 4 & 4 & 4 \\ 4 & 4 & 4 & 4 & 4 & 4 & 4 & 4 & 4 & 4 \\ 4 & 4 & 4 & 5 & 5 & 5 & 5 & 5 & 5 & 5 \\ 5 & 5 & 5 & 5 & 5 & 5 & 5 & 5 & 5 & 5 \end{bmatrix}$$

The process of this algorithm converges in 20 minutes, and the results are shown in Fig. 7. After the optimization, the anomalous high side lobes of the scattering pattern are uniformly reduced to low levels. Figure 8(a) schematically shows the optimized MSS, where super element of 2×2 same meta-atoms is utilized to better satisfy the periodic hypothesis in the element analysis. Consider the high nonlinearity and complexity of this problem, the optimal solutions may be not unique. Since the transmission wave is totally blocked by the metasurface ground, the EM wave absorption are only related to the reflection, which is calculated as $A(f) = 1-R(f)$. Here, $A(f)$ is the power absorption rate as a function of frequency, and $R(f)$ is the total scattering power of the whole backward half-space calibrated to that from the same-sized metallic plate. In detail, this calibration can be expressed as:

$$R = \frac{\iint \frac{1}{2}\mathrm{Re}(\overrightarrow{E_s} \times \overrightarrow{H_s}) \cdot \overrightarrow{\mathrm{d}s}}{\iint \frac{1}{2}\mathrm{Re}(\overrightarrow{E_{sm}} \times \overrightarrow{H_{sm}}) \cdot \overrightarrow{\mathrm{d}s}} \tag{11}$$

where $\overrightarrow{E_s}$ and $\overrightarrow{H_s}$ are the scattered electric field and magnetic field from MSS, while $\overrightarrow{E_{sm}}$ and $\overrightarrow{H_{sm}}$ are those from the same-sized metallic plate. In other words, by integrating all the scattering energy in the upper half space and comparing with that from the same-sized conducting plate, we can obtain the EM wave absorption by the MSS which ensures a high efficient ultra-wide bandwidth absorption from 3.74 to 18 GHz.

V. EXPERIMENTAL VERIFICATION

To verify the feasibility and practicality of the MSS, a prototype is fabricated. Resistive ink made of graphite powders is used for fabricating the resistive sheet with surface impedance approximating 377Ω/□ (with a tolerance of ±5%). The reflective metasurface is fabricated on a 3 mm thick FR4 substrate with relative permeability of 4.3 and loss tangent of about 0.002. The air spacer is mimicked by a microwave foam slab with 6 mm thickness. Figure 8(b) and 8(c) show the photograph of the metasurface and resistive film.

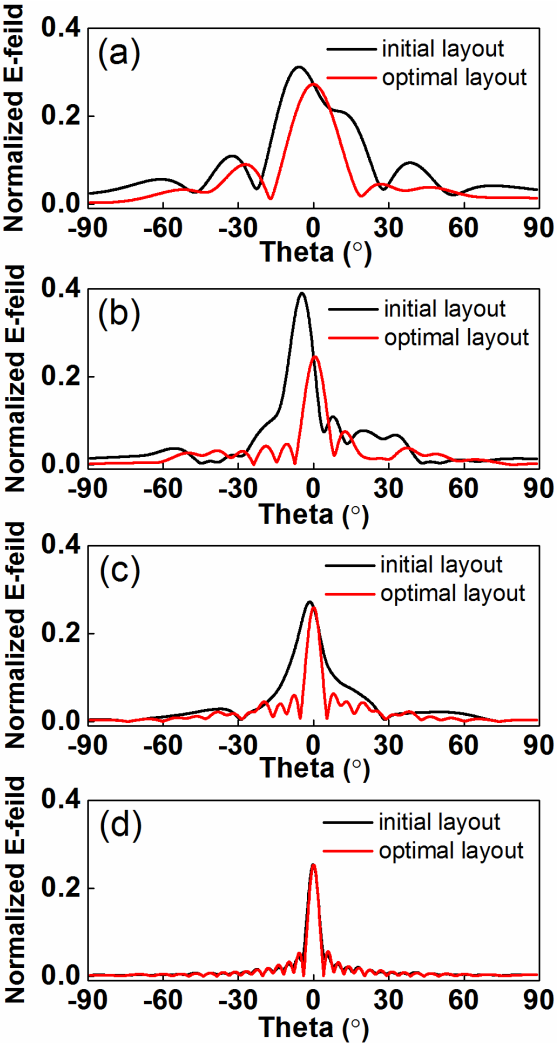

FIGURE 7. The normalized scattering patterns of the MSS with and without optimization at (a) (a) 4 GHz, (b) 9 GHz, (c) 14 GHz, and (d) 19 GHz.

In the experiment set-up, two horn antennas, with one severing as the emitter and the other as detector, are connected to the vector network analyzer. The reflection performance of the MSS is calibrated to a metallic slab with same size. The scattering energy to the upper half space is measured to calculate the EM wave absorption of the MSS. The energy absorption of the sample illuminated by the normal incidence with x- and y-polarization are shown in Fig. 9(a) and 9(b), respectively. The measured results are roughly in coincidence with the simulated and theoretical results, exhibiting an 88%

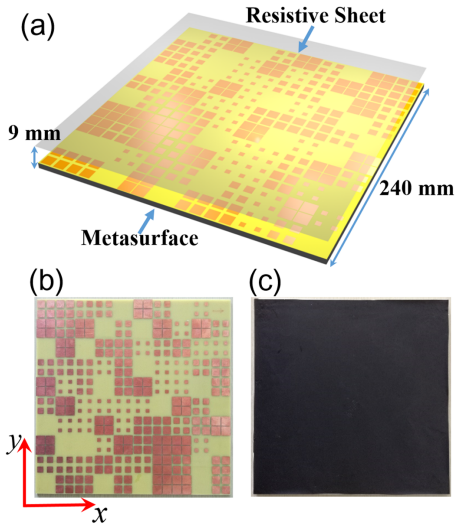

FIGURE 8. (a) Schematic of proposed MSS with optimized layout. (b) Photograph of the fabricated metasurface. (c) Photograph of the printed resistive sheet.

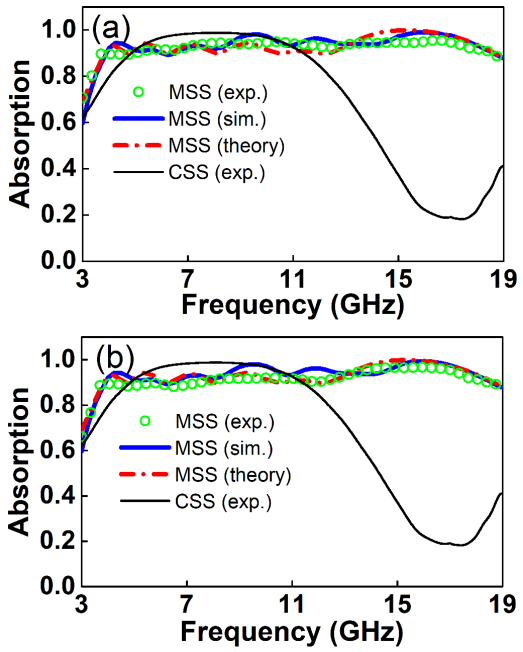

FIGURE 9. Theoretical, simulated and measured absorption performance of MSS with (a) *x*-polarized, (b) *y*-polarized normal incidence.

high absorption from 3.74 GHz to 18.5 GHz for both TE and TM polarizations. The broad absorption band is attributed to the closely distributed neighboring MSS resonances, which can be evidenced by the variation in the absorption curves. Compared with the CSS of the same thickness ($l = 9$ mm), the MSS shows a significant improvement in the relative absorption bandwidth (with respect to the center frequency), where the bandwidth defined by over 88% absorption is improved from 83% (CSS) to 133% (MSS), clearly validating the concept of MSS serving as an ultra-wideband

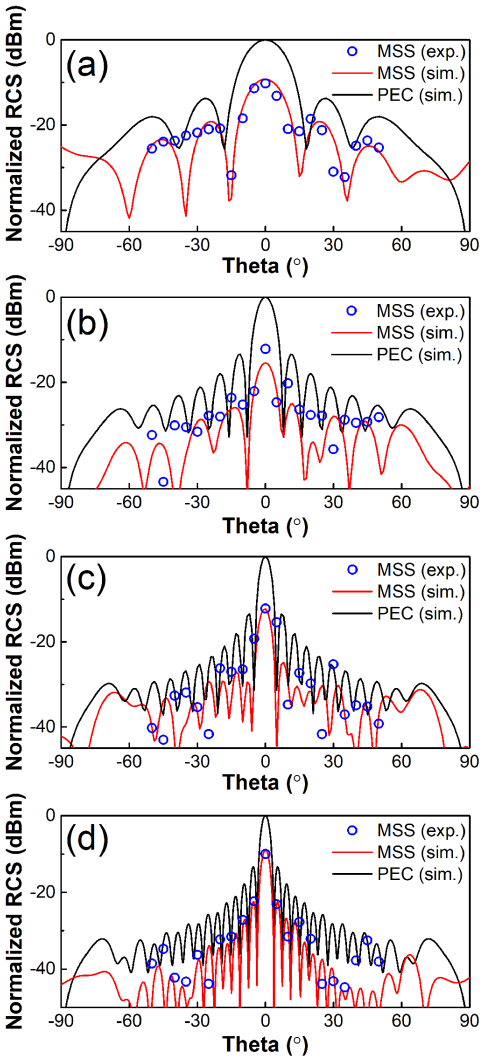

FIGURE 10. Far-field scattering patterns of the MSS at (a) 4 GHz, (b) 9 GHz, (c) 14 GHz, and (d) 19 GHz, with calibrated to the backward RCS of the metallic plate.

EM absorber. Gradient or non-periodic spatial arrangement is often adopted in the newly developed metasurface, while periodic hypothesis is often used as the approximation in the element design and analysis [46]–[50]. Also, the edge effects and the mutual coupling are disregarded for the analytical model, and the imperfection of the printed resistive sheet may lead to its real surface impedance not being exactly 377Ω/□. These, more or less, will lead to some differences between theoretical and experimental results [51]. However, the absorption bandwidth of these results are in good agreements. Thus, the theoretical analysis and optimization method could still allow a simple, fast and efficient design of ultra-wide band EM absorbers without reliance on the full-wave simulation.

The RCS can be suppressed in the whole backward half-space due to the absorption of the MSS, which can be seen in the far-field scattering patterns of the MSS measured and then

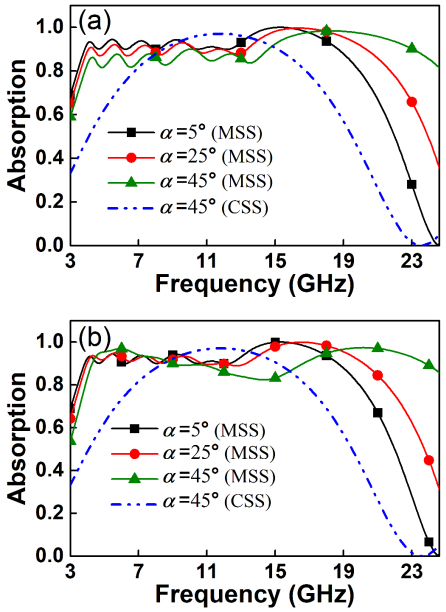

FIGURE 11. The theoretically calculated absorptions of MSS and CSS under oblique incidence with (a) TE polarization and (b) TM polarization.

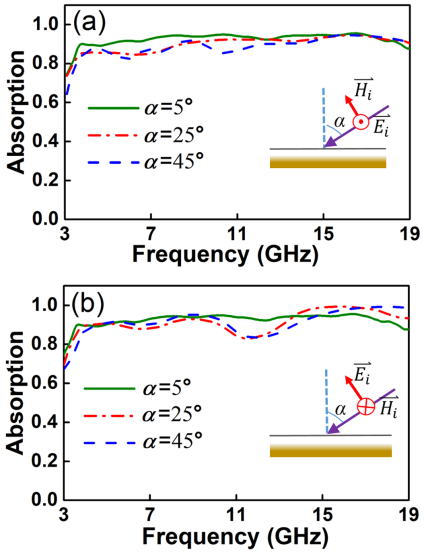

FIGURE 12. The measured absorption under oblique incidence with (a) TE polarization and (b) TM polarization. Insets show the corresponding definition of TE and TM mode.

compared with that of metallic plate in Fig. 10. An appreciable RCS reduction can be achieved at most directions both in simulated and measured results of $\boldsymbol{E}$-plane scattering pattern. The full wave simulations and experiments are in good coincidence, and both of them demonstrate the good performance of the proposed MSS. Since the side-lobes of scattering pattern are negligible compared to that of the dominating lobe at $\theta = 0°$, these results also confirm that the algorithm mentioned above to optimize the spatial arrangement of the MSS elements is quite efficient.

The power absorption of the proposed MSS for oblique incidence can be calculated by varying incident angle α in our framework of theory. The robust angular stability is an important criterion to evaluate the absorber for practical uses. The absorption performance of the MSS for oblique incidence can be readily calculated by varying incident angle α in our framework of theory. First, the scattered field of the whole back space is evaluated by considering the element spatial distribution and the reflection coefficient $\Gamma(f; w_i; \alpha)$ of the MSS elements. Here, $\Gamma(f; w_i; \alpha)$ is the reflection coefficient of MSS element under oblique incidence with an incident angle α, which can be calculated by equations (2), (3) and (6) for both TE and TM polarizations. Then, by summing up the total scattering field in the whole backward half-space and applying the aforementioned formula $A(f) = 1 - R(f)$, the power absorption for oblique incidence can be obtained.

The calculated results in Fig. 11 show that absorption efficiency over 82% from 4 GHz to 19 GHz can be well achieved till the incident angle up to about 45° for both TE and TM polarizations. The measured results for oblique incidence are displayed in Fig. 12, which agree roughly with that of the theoretical calculations. For the CSS, as the increase of the incident angle, the working band shifts towards higher frequency, accompanied by the absorption being less-efficiency, while for the proposed MSS, the MSS elements have a better angular stability especially in low frequency region as discussed in the previous section, and the multiple closely distributed resonances can ensure a broad operation band. Since the second MSS resonance shifts towards higher frequency as the incident angle gradually increases, the MSS even has a broader bandwidth but with a little less efficiency for large incident angles. Based on these results, it concludes that the robust angular performance of the MSS can be obtained by employing the metasurface ground.

The recently proposed diffusion metasurfaces have similar EM functionalities when compared with the absorbers in application to the reduction of the backward scattering of targets, but with quite different working mechanisms. In a diffusion metasurface, there is little energy absorption during the wave coupling and reflection, and the impinging energy is just randomly reflected into many directions [37]–[40]. Meanwhile, an absorber can efficiently dissipate the incoming wave by the lossy materials or its structural resonances to ensure an ultra-low scattering in all directions. In our scenario, the metasurface ground is designed to excite multiple and closely-distributed MSS resonances, ensuring that the incident energy can be efficiently dissipated as ohmic loss.

The recent research reveals the existence of theoretical minimum thickness $d_{\min}$ of an absorber with given bandwidth and absorption efficiency [6]. In order to evaluate the comprehensive performance of the proposed MSS, we calculate the $d_{\min}$ of the fabricated sample, given by [6]:

$$d_{\min} = \frac{\left| \int_0^{\infty} \ln |R(\lambda)| \, \mathrm{d}\lambda \right|}{2\pi^2} \tag{12}$$

TABLE 1. Comparison with other absorbers.

Absorber	Bandwidth	Thickness
[14]	131.6% 3.3-16 GHz (Sim.)	0.169λ
[16]	109.8% 6.7-23 GHz (Sim.)	0.112λ
[24]	129% 1.97-9.2 GHz (Exp.)	0.087λ
[23]	63% 7.7-14.8 GHz (Exp.)	0.128λ
This work	132.7% 3.74-18.5 GHz (Exp.)	0.112λ

where $R(\lambda)$ denotes the reflection coefficient as a function of the wavelength. The ultimate thickness for the proposed MSS is about 6.84 mm, approximate 76% of the thickness of the fabricated prototype, showing improvement compared with the previous one [35].

The proposed MSS absorber is compared with some of the representative previous works, including Jaumann Screens [14], CA absorbers loaded with either high impedance surface [16] or lumped elements [24], and multi-layered metamaterial absorber [23]. Here, the relative thickness is referred to the wavelength of the lowest operation frequency, and the bandwidth is defined by absorption over 88% (backward RCS reduction over 9.5 dB). As shown in Table 1, the proposed MSS can provide an ultra-wide absorption bandwidth with a relatively low profile. Besides, the MSS has other advantages such as extremely simple configuration and light weight, easy and fast design by employing the proposed systematic optimization algorithms.

VI. CONCLUSION

In conclusion, we analyze the MSS element with an accurate equivalent circuit model either for normal or oblique incidence, and then develop a systematic and efficient method for designing MSS absorber in microwave range. The MSS absorber are based on a metasurface ground with extremely simple patch pattern, and the resonant feature of the MSS element can be flexibly controlled by tuning the metasurface geometries. Based on these, GA and simulated annealing algorithm are carried out to efficiently optimize the MSS element geometries and their spatial distribution. The experimental results show that the MSS with high absorption over 88% from 3.74 GHz to 18.5 GHz can be achieved under the normal incidence with either x- or y-polarization, demonstrating a significant improvement over the CSS with operation band only from 4.8 GHz to 11.5 GHz. Moreover, the robust angular stability is demonstrated both in the theoretical analysis and experiment. It should be addressed that the design principle could be extended to higher frequency bands, such as THz and the IR regimes [52], and the proposed MSS has promising potentials in many applications such as electromagnetic compatibility, stealth technique, etc.

ACKNOWLEDGMENT

Ziheng Zhou would like to thank Li Cui's careful help in the full wave simulation and experimental measurement, and Yijing He's help in editing the Table 1.

REFERENCES

[1] C. M. Watts, X. Liu, and W. J. Padilla, "Metamaterial electromagnetic wave absorbers," *Adv. Mater.*, vol. 24, no. 23, pp. OP98–OP120, 2012.
[2] Y. Ra'di, C. R. Simovski, and S. A. Tretyakov, "Thin perfect absorbers for electromagnetic waves: Theory, design, and realizations," *Phys. Rev. Appl.*, vol. 3, no. 3, p. 37001, 2015.
[3] E. F. Knott, J. F. Shaeffer, and M. T. Tuley, *Radar Cross Section: Its Prediction, Measurement and Reduction*. Dedham, MA, USA: Artech House, 1985.
[4] K. J. Vinoy and K. M. Jha, *Radar Absorbing Materials*. Dordrecht, The Netherland: Kluwer, 1996.
[5] S. Genovesi, F. Costa, and A. Monorchio, "Wideband radar cross section reduction of slot antennas arrays," *IEEE Trans. Antennas Propag.*, vol. 62, no. 1, pp. 163–173, Jan. 2014.
[6] K. N. Rozanov, "Ultimate thickness to bandwidth ratio of radar absorbers," *IEEE Trans. Antennas Propag.*, vol. 48, no. 8, pp. 1230–1234, Aug. 2000.
[7] D. L. Jaggard, N. Engheta, and J. Liu, "Chiroshield: A Salisbury/Dallenbach shield alternative," *Electron. Lett.*, vol. 26, no. 17, pp. 1332–1334, Aug. 1990.
[8] G. Ruck, D. E. Barrick, W. D. Stuart, and C. K. Krichbaum, *Radar Cross Section Handbook*. New York, NY, USA: Plenum, 1970.
[9] W. W. Salisbury, "Absorbent body of electromagnetic waves," U.S. Patent 2 599 944A, Jun. 10, 1952.
[10] R. L. Fante and M. T. McCormack, "Reflection properties of the Salisbury screen," *IEEE Trans. Antennas Propag.*, vol. AP-36, no. 10, pp. 1443–1454, Oct. 1988.
[11] L. J. D. Toit, "The design of Jauman absorbers," *IEEE Antennas Propag. Mag.*, vol. 36, no. 6, pp. 17–25, Dec. 1994.
[12] L. J. D. Toit and J. H. Cloete, "Electric screen Jauman absorber design algorithms," *IEEE Trans. Microw. Theory Techn.*, vol. 44, no. 12, pp. 2238–2245, Dec. 1996.
[13] E. F. Knott and C. D. Lunden, "The two-sheet capacitive Jaumann absorber," *IEEE Trans. Antennas Propag.*, vol. 43, no. 1, pp. 1339–1343, Nov. 1995.
[14] A. Kazemzadeh and A. Karlsson, "Multilayered wideband absorbers for oblique angle of incidence," *IEEE Trans. Antennas Propag.*, vol. 58, no. 11, pp. 3637–3646, Nov. 2010.
[15] B. Munk, *Frequency Selective Surfaces: Theory and Design*. New York, NY, USA: Wiley, 2000.
[16] F. Costa, A. Monorchio, and G. Manara, "Analysis and design of ultra thin electromagnetic absorbers comprising resistively loaded high impedance surfaces," *IEEE Trans. Antennas Propag.*, vol. 58, no. 5, pp. 1551–1558, May 2010.
[17] S. Chakravarty, R. Mittra, and N. R. Williams, "On the application of the microgenetic algorithm to the design of broad-band microwave absorbers comprising frequency-selective surfaces embedded in multilayered dielectric media," *IEEE Trans. Microw. Theory Techn.*, vol. 49, no. 6, pp. 1050–1059, Jun. 2001.
[18] B. A. Munk, P. Munk, and J. Pryor, "On designing Jaumann and circuit analog absorbers (CA absorbers) for oblique angle of incidence," *IEEE Trans. Antennas Propag.*, vol. 55, no. 1, pp. 186–193, Jan. 2007.
[19] F. Costa and A. Monorchio, "Multiband electromagnetic wave absorber based on reactive impedance ground planes," *IET Microw., Antennas Propag.*, vol. 4, no. 11, pp. 1720–1727, Nov. 2010.
[20] D. Sievenpiper, L. Zhang, R. F. J. Broas, N. G. Alexopolous, and E. Yablonovitch, "High-impedance electromagnetic surfaces with a forbidden frequency band," *IEEE Trans. Microw. Theory Techn.*, vol. 47, no. 11, pp. 2059–2074, Nov. 1999.
[21] N. I. Landy, S. Sajuyigbe, J. J. Mock, D. R. Smith, and W. J. Padilla, "Perfect metamaterial absorber," *Phys. Rev. Lett.*, vol. 100, p. 207402, May 2008.
[22] N. Engheta, "Thin absorbing screens using metamaterial surfaces," in *Proc. Antennas Propag. Soc. Int. Symp.*, vol. 2, Jun. 2002, pp. 392–395.
[23] F. Ding, Y. Cui, X. Ge, Y. Jin, and S. He, "Ultra-broadband microwave metamaterial absorber," *Appl. Phys. Lett.*, vol. 100, no. 10, pp. 103504–103506, 2012.

[24] Y. Shang, Z. Shen, and S. Xiao, "On the design of single-layer circuit analog absorber using double-square-loop array," *IEEE Trans. Antennas Propag.*, vol. 61, no. 12, pp. 6022–6029, Dec. 2013.
[25] X. Huang, X. He, L. Guo, Y. Yi, B. Xiao, and H. Yang, "Analysis of ultra-broadband metamaterial absorber based on simplified multi-reflection interference theory," *J. Opt.*, vol. 17, no. 5, p. 55101, 2015.
[26] C. Mias and J. H. Yap, "A varactor-tunable high impedance surface with a resistive-lumped-element biasing grid," *IEEE Trans. Antennas Propag.*, vol. 55, no. 7, pp. 1955–1962, Jul. 2007.
[27] N. Yu *et al.*, "Light propagation with phase discontinuities: Generalized laws of reflection and refraction," *Science*, vol. 334, no. 6054, pp. 333–337, Oct. 2011.
[28] X. Ma, C. Huang, M. Pu, C. Hu, Q. Feng, and X. Luo, "Multi-band circular polarizer using planar spiral metamaterial structure," *Opt. Exp.*, vol. 20, no. 14, pp. 16050–16058, Jul. 2012.
[29] H. Chen *et al.*, "Ultra-wideband polarization conversion metasurfaces based on multiple plasmon resonances," *J. Appl. Phys.*, vol. 115, no. 15, p. 154504, 2014.
[30] M. Kenney, J. Grant, Y. D. Shah, I. Escorcia-Carranza, M. Humphreys, and D. R. S. Cumming, "Octave-spanning broadband absorption of terahertz light using metasurface fractal-cross absorbers," *ACS Photon.*, vol. 4, no. 10, pp. 2604–2612, 2017.
[31] X. Ni, S. Ishii, A. V. Kildishev, and V. M. Shalaev, "Ultra-thin, planar, babinet-inverted plasmonic metalenses," *Light Sci. Appl.*, vol. 2, no. 4, p. e72, 2013.
[32] K. Chen *et al.*, "A reconfigurable active huygens' metalens," *Adv. Mater.*, vol. 29, no. 17, pp. 1–20, 2017.
[33] S. Sun, Q. He, S. Xiao, Q. Xu, X. Li, and L. Zhou, "Gradient-index metasurfaces as a bridge linking propagating waves and surface waves," *Nature Mater.*, vol. 11, no. 5, pp. 426–431, 2012.
[34] X. Ni, Z. J. Wong, M. Mrejen, Y. Wang, and X. Zhang, "An ultrathin invisibility skin cloak for visible light," *Science*, vol. 349, no. 6254, pp. 1310–1314, 2015.
[35] Z. H. Zhou *et al.*, "Metasurface salisbury screen: Achieving ultra-wideband microwave absorption," *Opt. Exp.*, vol. 25, no. 24, p. 30241, 2017.
[36] A. K. Zadeh and A. Karlsson, "Capacitive circuit method for fast and efficient design of wideband radar absorbers," *IEEE Trans. Antennas Propag.*, vol. 57, no. 8, pp. 2307–2314, Aug. 2009.
[37] H. T. Chen, A. J. Taylor, and N. Yu, "A review of metasurfaces: Physics and applications," *Rep. Prog. Phys.*, vol. 79, no. 7, p. 76401, 2016.
[38] S. B. Glybovski, S. A. Tretyakov, P. A. Belov, Y. S. Kivshar, and C. R. Simovski, "Metasurfaces: From microwaves to visible," *Phys. Rep.*, vol. 634, pp. 1–72, May 2016.
[39] A. Fallahi, A. Yahaghi, H.-R. Benedickter, H. Abiri, M. Shahabadi, and C. Hafner, "Thin wideband radar absorbers," *IEEE Trans. Antennas Propag.*, vol. 58, no. 12, pp. 4051–4058, Dec. 2010.
[40] O. Luukkonen *et al.*, "Simple and accurate analytical model of planar grids and high-impedance surfaces comprising metal strips or patches," *IEEE Trans. Antennas Propag.*, vol. 56, no. 6, pp. 1624–1632, Jun. 2008.
[41] C. A. Balanis, *Antenna Theory: Analysis and Design*. New York, NY, USA: Wiley, 1997.
[42] D. Whitley, "A genetic algorithm tutorial," *Statist. Comput.*, vol. 4, no. 2, pp. 65–85, Jun. 1994.
[43] D. J. Kern and D. H. Werner, "A genetic algorithm approach to the design of ultra-thin electromagnetic bandgap absorbers," *Microw. Opt. Technol. Lett.*, vol. 38, no. 1, pp. 61–64, Jul. 2003.
[44] B. Schnetzler, "Optimization by simulated annealing," *Science*, vol. 220, no. 4598, pp. 671–680, 1992.
[45] J. Diao, J. W. Kunzler, and K. F. Warnick, "Sidelobe level and aperture efficiency optimization for tiled aperiodic array antennas," *IEEE Trans. Antennas Propag.*, vol. 65, no. 12, pp. 7083–7090, Dec. 2017.
[46] K. Chen, L. Cui, Y. Feng, J. Zhao, T. Jiang, and B. Zhu, "Coding metasurface for broadband microwave scattering reduction with optical transparency," *Opt. Exp.*, vol. 25, no. 5, pp. 5571–5579, 2017.
[47] K. Chen *et al.*, "Geometric phase coded metasurface: From polarization dependent directive electromagnetic wave scattering to diffusion-like scattering," *Sci. Rep.*, vol. 6, Oct. 2016, Art. no. 35968.
[48] L. Liang *et al.*, "Anomalous terahertz reflection and scattering by flexible and conformal coding metamaterials," *Adv. Opt. Mater.*, vol. 3, no. 10, pp. 1374–1380, 2015.
[49] L.-H. Gao *et al.*, "Broadband diffusion of terahertz waves by multi-bit coding metasurfaces," *Light Sci. Appl.*, vol. 4, no. 9, p. e324, 2015.
[50] T. J. Cui, M. Q. Qi, X. Wan, J. Zhao, and Q. Cheng, "Coding metamaterials, digital metamaterials and programmable metamaterials," *Light Sci. Appl.*, vol. 3, no. 10, p. e218, 2014.
[51] J. Diao and K. F. Warnick, "Antenna loss and receiving efficiency for mutually coupled arrays," *IEEE Trans. Antennas Propag.*, vol. 65, no. 11, pp. 5871–5877, Nov. 2017.
[52] S. J. Min *et al.*, "Tunable large resonant absorption in a midinfrared graphene Salisbury screen," *Phys. Rev. B, Condens. Matter*, vol. 90, no. 16, p. 165409, 2013.

ZIHENG ZHOU received the B.S degree in physics from Nanjing University, Nanjing, China, in 2017. He is currently pursuing the Ph.D. degree in electromagnetic field and microwave engineering with the Department of Electronic Engineering, Tsinghua University, Beijing, China.

His research interests include metamaterial/metasurface, antenna, and quantum physics in 2-D material.

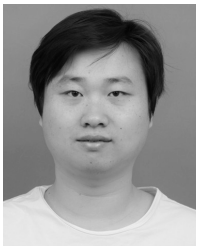

KE CHEN (M'17) received the B.S. and Ph.D. degrees in electronic science and engineering from Nanjing University, Nanjing, China, in 2012 and 2017, respectively.

He is currently a Post-Doctoral Fellow with the Department of Electronic Engineering, School of Electronic Science and Engineering, Nanjing University. His research interests include electromagnetic metamaterials and metasurfaces, and their applications to novel microwave functional devices.

BO ZHU (M'14) received the Ph.D. degree in electrical engineering from Nanjing University, Nanjing, China, in 2010.

In 2009, he was a Visiting Student with the Department of RF and Optical, Institute for Infocomm Research, Singapore. From 2010 to 2012, he was a Post-Doctoral Researcher with the Department of Electrical and Electronic Engineering, The University of Hong Kong, Hong Kong. Since 2012, he has been an Associate Researcher with the School of Electronic Science and Engineering, Nanjing University. His research interests include electromagnetics, metasurfaces, antennas, and electromagnetic compatibility devices.

Dr. Zhu is a member of the IEEE Antennas and Propagation Society. He also serves as the Reviewer of electromagnetics-related primary journals, including the IEEE TRANSACTIONS ON ANTENNAS AND PROPAGATION, *Advanced Materials Series*, OSA journals, *IET Microwaves, Antennas and Propagation*, and *Chinese Physics B*.

JUNMING ZHAO (M'17) received the B.S. and Ph.D. degrees in electronic science and engineering from Nanjing University, Nanjing, China, in 2003 and 2009, respectively.

Since 2009, he has been a Faculty Member with the Department of Electronic Engineering, School of Electronic Science and Engineering, Nanjing University, where is currently an Associate Professor. From 2014 to 2015, he was a Visiting Scholar with the Group of Antennas and Electromagnetics, School of Electronic Engineering and Computer Science, Queen Mary College, University of London. His research interests include electromagnetic metamaterials and metasurfaces, and their applications to novel microwave functional devices.

YIJUN FENG (M'97) received the M.Sc. and Ph.D. degrees from the Department of Electronic Science and Engineering, Nanjing University, in 1989 and 1992, respectively. Since 1992, he has been a Faculty Member with the Department of Electronic Engineering, School of Electronic Science and Engineering, Nanjing University, where he is currently a Full Professor.

From 1995 to 1996, he was a Visiting Scientist with the Physics Department, Technical University of Denmark. From 2001 to 2002, he was a Visiting Researcher with the University of California at Berkeley. He has authored or co-authored over 160 journal papers and over 120 referred international conference papers. His research interests include electromagnetic metamaterial and application to microwave and photonic devices, electromagnetic wave theory, and novel microwave functional materials. He has conducted over 20 scientific research projects, including the National 973, 863 Projects, and the National Natural Science Foundation Projects in China. He has received the 2010 Science and Technology Award (First Grade) of Jiangsu Province, China, and the 1995 Scientific and Technological Progress Award by the Minister of Education, China.

YUE LI (S'11–M'12–SM'17) received the B.S. degree in telecommunication engineering from the Zhejiang University, Zhejiang, China, in 2007, and the Ph.D. degree in electronic engineering from Tsinghua University, Beijing, China, in 2012.

He was a Visiting Scholar with the Institute for Infocomm Research, A*STAR, Singapore, in 2010, and the Hawaii Center of Advanced Communication, University of Hawaii at Manoa, Honolulu, HI, USA, in 2012. In 2012, he was a Post-Doctoral Fellow with the Department of Electronic Engineering, Tsinghua University. In 2013, he was a Research Scholar with the Department of Electrical and Systems Engineering, University of Pennsylvania. Since 2016, he has been with Tsinghua University, where he is currently an Associate Professor with the Department of Electronic Engineering. He has authored and co-authored over 80 journal papers and 30 international conference papers. He holds 15 granted Chinese patents. His current research interests include metamaterials, plasmonics, electromagnetics, nanocircuits, mobile and handset antennas, MIMO and diversity antennas, and millimeter-wave antennas and arrays.

He was a recipient of the Principal Scholarship of Tsinghua University in 2011, the Outstanding Doctoral Dissertation of Beijing Municipality in 2013, the Young Scientist Award from URSI General Assembly in 2014, the Young Scientist Award from URSI AP-RASC in 2016, the Young Scientist Award from EMTS in 2016, the Best Student Paper Award from ICMMT in 2016, the Best Paper Award from ISAPE in 2016, the Issac Koga Gold Medal from URSI General Assembly in 2017, and the Best Student Paper Award (Third Prize) from APCAP in 2017. He served as the Associate Editor for the IEEE TRANSACTIONS ON ANTENNAS AND PROPAGATION and the IEEE ANTENNAS AND WIRELESS PROPAGATION LETTERS.